Rac1 orientates epithelial apical polarity through effects on basolateral laminin assembly

Lucy Erin O'Brien*, Tzuu-Shuh Jou†¶, Anne L. Pollack‡, Qihang Zhang§, Steen H. Hansen*#, Peter Yurchenco§ and Keith E. Mostov***

**Department of Anatomy, Department of Biochemistry and Biophysics, and the Cardiovascular Research Institute, University of California, San Francisco, California 94143, USA*

†Department of Molecular and Cellular Physiology, Stanford University Medical School, Stanford, California 94305, USA

‡Department of Cell Biology and Anatomy, University of Arizona Health Sciences Center, Tucson, Arizona 85724, USA

§Department of Pathology, Robert Wood Johnson Medical School, Piscataway, New Jersey 08854, USA

¶Present address: Graduate Institute of Clinical Medicine, College of Medicine, National Taiwan University, and Department of Internal Medicine, National Taiwan University Hospital, Taipei, 100 Taiwan

#Present address: Boston Biomedical Research Institute, Watertown, Massachusetts 02472, USA

***e-mail: mostov@itsa.ucsf.edu*

Cellular polarization involves the generation of asymmetry along an intracellular axis. In a multicellular tissue, the asymmetry of individual cells must conform to the overlying architecture of the tissue. However, the mechanisms that couple cellular polarization to tissue morphogenesis are poorly understood. Here, we report that orientation of apical polarity in developing Madin–Darby canine kidney (MDCK) epithelial cysts requires the small GTPase Rac1 and the basement membrane component laminin. Dominant-negative Rac1 alters the supramolecular assembly of endogenous MDCK laminin and causes a striking inversion of apical polarity. Exogenous laminin is recruited to the surface of these cysts and rescues apical polarity. These findings implicate Rac1-mediated laminin assembly in apical pole orientation. By linking apical orientation to generation of the basement membrane, epithelial cells ensure the coordination of polarity with tissue architecture.

Cellular polarization is a two-stage process. First, cells select an axis of polarization in response to spatial cues. Second, cells generate molecular asymmetry along this selected axis[1]. In multicellular tissues, the axis of each polarized cell must be aligned with the overall structure of the tissue to achieve the specific geometry needed for tissue function. However, little is understood about the molecular mechanisms that couple polarity to tissue architecture.

Most epithelial organs consist of monolayers of cells that adhere to each other through cell–cell junctions. These monolayers are arranged in follicular or tubular structures that enclose a central lumen and are surrounded by a basement membrane. Individual epithelial cells establish the apical domain next to the lumen, indicating a link between cellular polarity and tissue structure. Indeed, cell–cell junctions, which are vital structural features of epithelia, direct apical polarization in invertebrates[2,3]. Mammalian epithelial cells grown on culture supports are able to form an apical domain in the absence of cell–cell junctions[4], indicating that a different cue might designate the apical pole under these circumstances. However, both the molecular nature of this cue and the basis of its coordination with epithelial architecture are unknown.

The extracellular matrix (ECM) represents a potential link between polarity and tissue organization. Dynamic cell–ECM interactions are integral to tissue morphogenesis, as illustrated by the reciprocal relationship between epithelia and their laminin-rich basement membrane. In developing epithelia, cells secrete laminin and assemble it into a polymeric network through the activity of cell-surface laminin receptors. Genetic or functional ablation of laminin receptors disrupts the process of laminin assembly and alters the appearance of laminin on the cell surface[5,6]. In explant culture and *in vivo*, assembled laminin provides morphogenetic signals essential for epithelial development[7–9]. Although the downstream effectors of laminin signalling are unknown, the asymmetric localization of laminin might indicate a role in polarization.

The prototype Rho family GTPases RhoA, Rac1 and Cdc42 propagate polarizing signals by inducing actin cytoskeletal remodelling at designated sites in the cell cortex. Mutations in these small GTPases cause loss or misorientation of polarity in diverse biological contexts. In the polarized Madin–Darby canine kidney (MDCK) epithelial cell line, expression of a dominant-negative allele of Cdc42 specifically depolarized basolateral membrane proteins[10]. By contrast, the expression of dominant-negative or constitutively active alleles of RhoA and Rac1 did not alter polarity despite effects on tight and adherens junctions[11–13]. These studies examined MDCK cells grown as monolayers on a synthetic support. The role of Rho-family GTPases in the three-dimensional organization of epithelial follicles and tubules has not yet been investigated.

How are cell polarity and tissue organization coupled during epithelial morphogenesis? To analyse this issue, we have examined the apical polarization of developing MDCK cysts embedded in ECM. Each cyst arises from the proliferation of a single cell to form a spherical monolayer of polarized cells enclosing a central lumen[14]. The organization of these cysts resembles that of epithelia *in vivo*, and thus cyst development provides a model system for the formation of a rudimentary epithelial suborgan[15]. Here we report that Rac1 and laminin form an autocrine pathway that orientates the apical pole during cyst development. Dominant-negative Rac1 impairs laminin assembly and strikingly inverts the apical pole to the cyst periphery. Exogenous laminin is recruited to the cyst surface and rescues apical polarity. By linking apical orientation to assembly of the basement membrane component laminin, our results illustrate how epithelia coordinate polarity with tissue architecture.

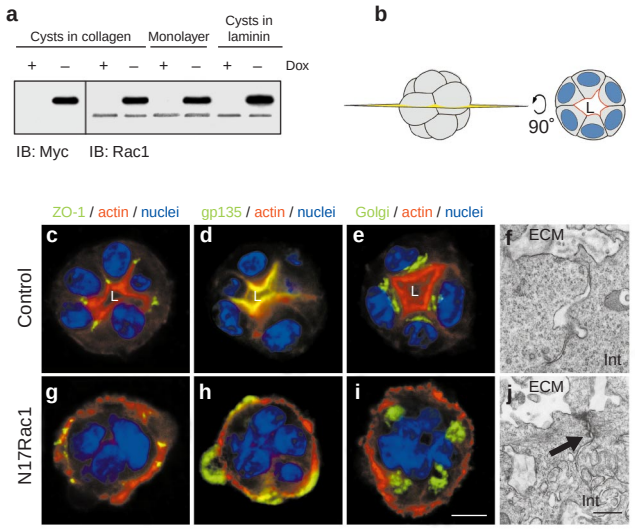

Figure 1 **N17Rac1 inverts apical polarity during cyst development.** **a**, Expression of exogenous and endogenous Rac1 in MDCK cells stably transfected with a vector encoding tetracycline-repressible Myc-N17Rac1. Cysts in collagen, monolayers on a filter support and cysts in laminin were harvested 4 days after plating. Lysates from each culture condition were immunoblotted (IB) with either an anti-Myc antibody, which detects only exogenous Myc-N17Rac1 (left two lanes), or an anti-Rac1 antibody, which detects both exogenous and endogenous Rac1 (right six lanes). The Myc tag retards the migration of exogenous N17Rac1 (upper band), permitting its distinction from endogenous Rac1 (lower band). Equal amounts of lysate were loaded in each lane. **b**, Schematic diagram of a typical cyst in ECM, exterior view (left) and cross-sectional view (right). The lumen (L), apical surface (red) and nuclei (blue) are shown. **c–e**, **g–i**, Immunocytochemical analysis of apical polarization in 4-day control and N17Rac1 cysts. Cysts are stained for apical domain markers (green), actin (red) and nuclei (blue). Localization of the tight-junction protein ZO-1, the apical plasma-membrane protein gp135, the *cis*-Golgi enzyme GM130 and intense actin staining reveals the establishment of the apical pole at the interior luminal surface of control cysts but at the periphery of N17Rac1 cysts. Although control cysts exhibit discernible lumina (L), N17Rac1 cysts do not. Scale bar, 10 μm. **f**, **j**, At the ultrastructural level, structures resembling tight junctions are present at the periphery of N17Rac1 cysts (arrow) but not control cysts. Red lines denote cyst boundaries; Int and ECM indicate cyst interiors and the extracellular matrix, respectively. Scale bar, 500 nm.

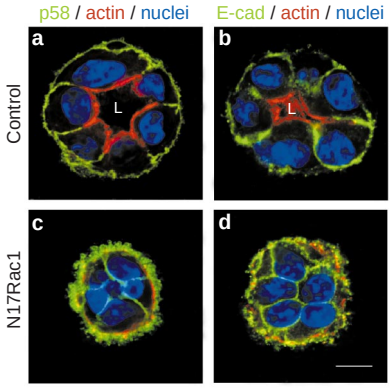

Figure 2 **Basolateral markers localize to all cell surfaces in N17Rac1 cysts.** Immunocytochemical analysis of basolateral polarization in 4-day control cysts (**a**, **b**) and N17Rac1 cysts (**c**, **d**). Cysts are stained for basolateral proteins (green), actin (red) and nuclei (blue). The basolateral markers p58 (**a**, **c**) and E-cadherin (**b**, **d**) localize to cell–cell and cell–ECM contacts in both control and N17Rac1 cysts. L, lumen. Scale bar, 10 μm.

Results

Dominant-negative Rac1 specifically inverts apical polarity. To examine the role of Rac1 during cyst morphogenesis, we used MDCK cell lines that conditionally expressed either dominant-negative (N17) or constitutively active (V12) Myc-tagged alleles of Rac1 under control of the tetracycline-repressible transactivator[12]. Cysts grown in collagen I, monolayers grown on filters, and cysts grown in laminin-1 all expressed exogenous Rac1 in the absence of doxycycline but not in the presence of 20 ng ml^{-1} doxycycline (Fig. 1a and not shown). In all assays, control cells grown in 20 ng ml^{-1} doxycycline behaved identically to untransfected MDCK cells.

We characterized apical polarization during normal cyst development by analysing single confocal optical sections taken through whole mounts of cysts grown, fixed and stained in collagen I gels (Fig. 1b). Virtually all 4-day control cysts established the apical pole in the cyst interior (96%, $n = 595$), as indicated by the localization of the tight-junction protein ZO-1, the apical plasma membrane protein gp135, the Golgi apparatus, and intense actin staining probably representing microvilli and the terminal web (Fig. 1c–e). Lumina were visible in 87% of the cysts ($n = 595$) and were invariably adjacent to the apical domain.

We next examined the development of cysts expressing either V12Rac1 or N17Rac1. Four-day V12Rac1 cysts seemed identical to control cysts except for an intensification of actin staining at the luminal surface. In contrast to the V12Rac1 cysts, four-day N17Rac1 cysts exhibited a specific inversion of the apical pole. The vast majority of N17Rac1 cysts established an apical pole at the cyst periphery (83%, $n = 657$), as evidenced by the localization of ZO-1, gp135, the Golgi apparatus, and intense actin staining (Fig. 1g–i). Ultrastructural analysis confirmed that the ZO-1 staining of N17Rac1 cysts represented apparent tight-junction formation (Fig. 1j). N17Rac1 cysts lacked lumina at both light-microscopic (Fig. 1g–i) and ultrastructural levels (not shown).

The inverted apical pole of N17Rac1 cysts exhibited some differences from the apical pole of control cysts. First, although actin filaments were concentrated at the N17Rac1 apical pole, they were not assembled into microvilli (not shown). Second, gp135 was detected in only 60% of peripheral cells in the N17Rac1 cysts ($n = 90$ cells from 14 different cysts). Often, gp135-positive regions of the plasma membrane seemed to protrude from the N17Rac1 cyst surface (Fig. 1h). Although actin also localized to the cyst periphery, it was largely excluded from these membrane protrusions.

To determine whether inverted apical polarity required continuous N17Rac1 expression, we cultured cysts without doxycycline for 4 days, during which they expressed N17Rac1 and misorientated the apical pole. We then repressed further N17Rac1 expression with 20 ng ml^{-1} doxycycline. Within 2 days of the addition of doxycycline, these cysts repolarized in the proper orientation and formed lumina (not shown). Thus, the inverted apical pole is subject to remodelling in response to restored Rac1 signalling.

We also examined basolateral polarization during cyst development (Fig. 2). The basolateral markers p58 and E-cadherin localized to surfaces of cell–cell and cell–substratum contact in both control and N17Rac1 cysts. In control cysts, these markers were excluded from the luminal surface (Fig. 2a, b). In N17Rac1 cysts, which lacked lumina, these markers were distributed over the entire plasma membrane (Fig. 2c, d). This nonpolar distribution could result from the absence of a luminal surface to exclude basolateral proteins. In fact, a similar overlap of basolateral markers with the apical pole occurs during early stages of normal MDCK morphogenesis, before the appearance of lumina[4,16–18]. It is also possible that N17Rac1 cysts have lost the ability to restrict basolateral markers.

In summary, the expression of constitutively active Rac1 did not significantly alter MDCK cyst morphogenesis. In contrast, expression of dominant-negative Rac1 caused a selective inversion of the

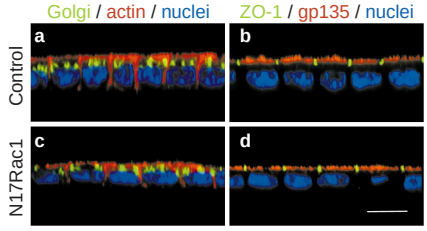

Figure 3 **N17Rac1 does not alter the polarity of monolayers.** Immunocytochemical analysis of apical polarization in 6-day control monolayers (**a**, **b**) and N17Rac1 monolayers (**c**, **d**). **a**, **c**, The *cis*-Golgi enzyme GM130 (green) and intense actin staining (red) are polarized toward the free upper surface of both control and N17Rac1 monolayers. **b**, **d**, The tight-junction protein ZO-1 (green) and the apical plasma membrane protein gp135 (red) are also polarized towards the upper surface of both monolayers. Nuclei are stained blue. Cells expressing N17Rac1 are consistently 3–4 μm shorter than control cells, as previously reported[12]. Scale bar, 10 μm.

apical pole to the cyst periphery, accompanied by a failure of lumen formation. The absence of lumina might explain why basolateral membrane proteins exhibit a nonpolar distribution in N17Rac1 cysts.

Extracellular environment modulates the polarity effects of N17Rac1. To investigate how the extracellular environment modulates the effects of N17Rac1, we examined the polarization of cells grown as a monolayer on a filter support and cysts grown in suspension. In both control and N17Rac1 monolayers, the localization of ZO-1, gp135, the Golgi apparatus and intense actin staining revealed the apical pole to be at the free cellular surface in contact with the medium (Fig. 3a–d). Thus, N17Rac1 did not alter apical polarization in monolayers despite expression levels comparable to those of collagen-grown cysts (Fig. 1a). When grown in suspension culture, MDCK cells form cysts with a cellular organization similar to that of cysts grown in ECM but with inverted polarity[19]. The apical pole of suspension-grown cysts faces the free cellular surface of the cyst periphery, and the basolateral pole faces the adhesive surfaces of the cyst interior. In suspension culture, N17Rac1 cysts orientated the apical pole at the cyst periphery, like control cysts (not shown). These findings indicate that Rac1 is specifically required for polarization of cysts in collagen.

N17Rac1 impairs laminin assembly at the cyst surface. Because the effects of N17Rac1 were manifested only in collagen culture, we hypothesized that impaired cell–ECM interactions formed the basis of the N17Rac1 cyst phenotype. Numerous studies implicating laminin in epithelial morphogenesis (reviewed in ref. 20) prompted us to examine levels of laminin in control and N17Rac1 cyst cultures. Although epithelia synthesize several types of laminin, the most studied is laminin-1, a trimer composed of the laminin α1 chain (relative molecular mass ~400,000 (M_r 400K)), β1 chain (M_r 210K) and γ1 chain (M_r 200K). MDCK cells might also express other variants of laminin, such as laminin-10, which have chains in common with laminin-1 and thus would have been detected by our polyclonal antibody against laminin-1.

To examine laminin in cyst-containing collagen gels, we used heat and detergent to solubilize the collagen I matrix and lyse the cysts. MDCK laminin was then detected through immunoprecipitation and immunoblotting, revealing a broad band that migrated with the unresolved β1/γ1 band of purified laminin-1 at M_r ~200K (Fig. 4a, and not shown). Additionally, immunoblotting inconsistently detected a slower band that migrated with the α1 chain of purified laminin-1 (not shown). The relative intensities of the α1 band and the β1/γ1 band were similar for control and N17Rac1 samples. Notably, solubilized control and N17Rac1 gels contained statistically indistinguishable amounts of laminin (Fig. 4a, d). We next examined laminin in the medium surrounding the gels by immunoprecipitation and immunoblotting. Again, control and N17Rac1 medium contained statistically similar amounts of laminin (Fig. 4c, d). The sum of laminin in the cyst-containing gel and the medium comprised the total laminin in the cyst culture. Thus, N17Rac1 does not alter the steady-state levels of total laminin.

We also quantified intracellular laminin levels to determine whether N17Rac1 altered laminin secretion. To isolate intact cysts, cyst cultures were digested with collagenase and then centrifuged gently. Both the supernatant (not shown) and the cyst pellet (Fig. 4b) contained laminin. As expected, the sum of these two fractions was comparable to the amount of laminin in solubilized, cyst-containing gels. The laminin associated with isolated cysts appeared as two species. The slower, more abundant species (Fig. 4b, asterisk) migrated with laminin from solubilized gel or medium. This species diminished when intact cysts were treated with trypsin, suggesting that it was extracellular. In contrast, the faster species (Fig. 4b, filled circle) was not detectable in solubilized gel or medium samples, probably because it comprised less than 1% of the total laminin in the culture (Fig. 4d). This species was resistant to trypsin, indicating that it might be intracellular. Its smaller size, low abundance and intracellular localization are consistent with that of a biosynthetic intermediate. Importantly, control and N17Rac1 cysts contained comparable levels of the intracellular laminin species (Fig. 4b, d), indicating that N17Rac1 does not alter laminin secretion.

The isolated N17Rac1 cysts possessed significantly higher levels of trypsin-sensitive, extracellular laminin (Fig. 4b, d). We therefore examined patterns of deposition of endogenous laminin by immunofluorescence. Laminin staining on the surface of control cysts was regular and punctate (Fig. 5a–c). No paracellular laminin staining was apparent. Projections of serial confocal sections demonstrated that the laminin puncta were distributed uniformly over the entire cyst surface (Fig. 5g). Although N17Rac1 cysts also exhibited no apparent paracellular laminin, their cell-surface laminin staining was markedly altered (Fig. 5d–f). Confocal projections revealed larger laminin patches, irregularly distributed on the N17Rac1 cysts (Fig. 5h).

The biochemical result that laminin levels were not decreased in N17Rac1 cyst cultures, combined with the abnormal appearance of laminin on the N17Rac1 cyst surface, is a strong indication that this laminin is misassembled. Specifically, it is well established that perturbation of the laminin assembly process alters laminin's immunofluorescent staining pattern, rendering it faint and/or disorganized[5,6,8,21]. These effects are similar to that seen on the N17Rac1 cyst surface. Although the precise relationship between the sparse laminin patches revealed by immunofluorescence (Fig. 5h) and the trypsin-sensitive cell-surface laminin (Fig. 4b) is currently unclear, we suspect that the misassembly of laminin on N17Rac1 cysts probably interfered with its immunocytochemical detection. For example, our anti-laminin antibody, raised against native laminin, might have recognized misassembled laminin inefficiently. Indeed, conformation-dependent reactivity of anti-laminin antibodies has been reported previously[22]. It is also possible that the laminin patches were incompletely penetrated by the antibody, or that their staining intensity saturated the linear range of the confocal microscope.

Cell-surface laminin receptors mediate the supramolecular assembly of laminin[5,6,23]. To investigate whether N17Rac1-induced laminin misassembly might be the consequence of altered receptor levels, we examined the three major MDCK laminin receptors: dystroglycan, $\alpha_6\beta_4$ integrin and $\alpha_3\beta_1$ integrin[24]. Control and N17Rac1 cysts exhibited comparable levels of α-dystroglycan (Fig. 4e), α_6 integrin, β_4 integrin and β_1 integrin (not shown) in immunoblots of isolated cysts. However, N17Rac1 cysts exhibited markedly decreased α_3 integrin levels (Fig. 4e; 32 ± 6% of control). Because

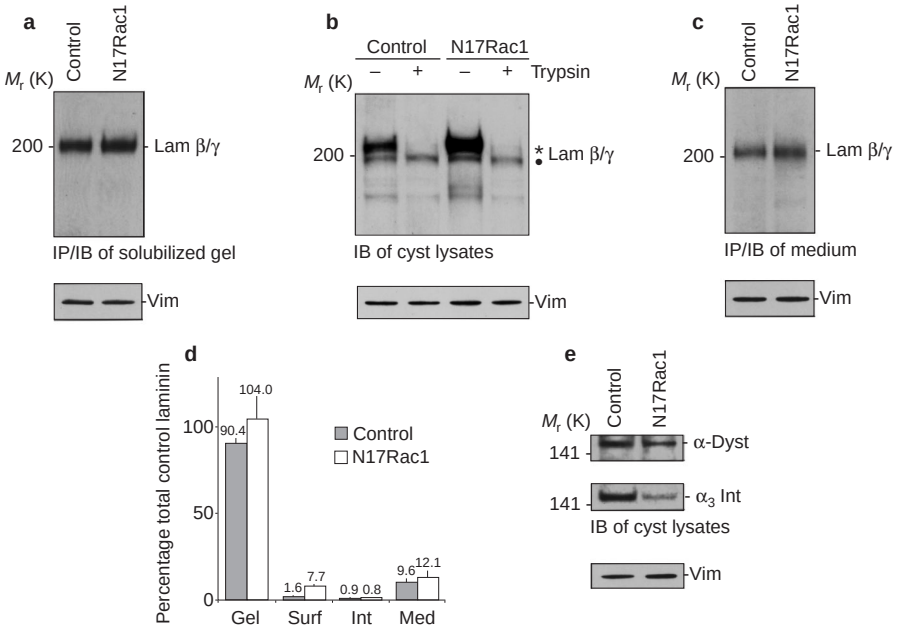

Figure 4 **N17Rac1 does not reduce laminin levels or inhibit laminin secretion. a**, Steady-state laminin levels are unchanged in N17Rac1 cyst cultures. Four-day control and N17Rac1 cyst cultures were solubilized and the cysts were lysed. The resulting mixture was immunoprecipitated (IP) and immunoblotted (IB) with an anti-laminin antibody that detects the laminin β1 and γ1 chains (Lam β/γ). A parallel immunoprecipitation/immunoblot of vimentin (Vim) verifies that an equal amount of lysate is represented in each lane. **b**, Intracellular laminin is unchanged, whereas cell-surface laminin is increased in isolated N17Rac1 cysts. Four-day control and N17Rac1 cysts were isolated from collagen gels by collagenase treatment and gentle centrifugation. To distinguish between extracellular and intracellular laminin, some intact cysts were also treated with trypsin before lysis. Cyst lysates were immunoblotted with anti-laminin antibody. The more slowly migrating, trypsin-sensitive laminin on the cyst surface is denoted by an asterisk; the faster migrating, trypsin-resistant, intracellular laminin is denoted by a filled circle. Lysates were also immunoblotted for vimentin to ensure equal loading. **c**, Laminin in the medium of N17Rac1 cyst cultures is unchanged. Medium from 4-day control and N17Rac1 cyst cultures were subjected to immunoprecipitation and immunoblotting with anti-laminin antibody. An immunoblot of vimentin from a parallel preparation of cyst lysates verifies that each lane represents medium conditioned by equal numbers of cells. **d**, Quantification of laminin in 4-day control and N17Rac1 cyst cultures. Immunoprecipitation and immunoblotting were performed to detect laminin in solubilized, cyst-containing collagen gels (Gel), trypsin-sensitive laminin on the surface of isolated cysts (Surf), trypsin-insensitive intracellular laminin (Int) and laminin in the medium (Med). Measurements of band intensity are presented as the percentage of total control laminin, which was designated as the sum of the laminin in solubilized gels and the laminin in the medium of control cultures. Results are means ± s.e.m. for three separate experiments. **e**, N17Rac1 cysts exhibit significantly decreased levels of the laminin receptor α_3 integrin. Four-day control and N17Rac1 cyst lysates were immunoblotted for the laminin receptors α-dystroglycan (α-Dyst), α_3 integrin (α_3 Int), α_6 integrin, β_1 integrin or β_4 integrin (not shown). In N17Rac1 cysts, levels of α_3 integrin were diminished to 32 ± 6% of control levels, whereas all other receptor levels remained similar. Lysates were also immunoblotted for vimentin to ensure equal loading.

$\alpha_3\beta_1$ integrin is required for laminin assembly[25], this decrease might represent the basis of N17Rac1-induced laminin misassembly.

In summary, we examined the quantitative and morphological effects of N17Rac1 on laminin. Steady-state levels of both intracellular and total laminin were comparable in N17Rac1 and control cyst cultures, indicating that laminin biosynthesis was not significantly altered by N17Rac1. However, the large-scale spatial organization of laminin on N17Rac1 cysts was grossly abnormal, perhaps owing to decreased levels of α_3 integrin. Taken together, these results imply that N17Rac1 alters the assembly of laminin on the cyst surface.

Exogenous laminin is sufficient to reorientate the apical pole. To test whether apical inversion was a downstream effect of laminin misassembly, we examined the ability of exogenous laminin to rescue N17Rac1 cyst polarity. The presence of purified laminin-1 (250 μg ml^{-1}) in the collagen I gel did not affect expression of the N17Rac1 transgene (Fig. 1a). In these mixed laminin-1/collagen I cultures, laminin appeared as a halo around both N17Rac1 and control cysts (Fig. 6e, and not shown). Confocal projections revealed this staining to include a diffusely bright signal and a punctate component (Fig. 6f); these puncta were reminiscent of laminin on control cysts in collagen I alone (Fig. 5g). The uniformity of this staining contrasted with the sparse appearance of endogenous laminin on N17Rac1 cysts in collagen I alone (Fig. 6a, b), suggesting that exogenous laminin was recruited to the N17Rac1 cyst surface.

Strikingly, exogenous laminin restored proper apical orientation to the N17Rac1 cysts. Most N17Rac1 cysts established the apical pole in the cyst interior, as revealed by staining for actin, ZO-1 and gp135 (Fig. 6g, h, k). The interior localization of these markers contrasts with their peripheral localization in N17Rac1 cysts in collagen I alone (Fig. 6c, d). N17Rac1 cysts in exogenous laminin typically contained lumina (84%, $n = 1,547$). Perhaps because compromised tight junctions inhibited their enlargement[13,26], N17Rac1 lumina were smaller and the incidence of multiple lumina was higher (24% of 2,062 N17Rac1 cysts compared with 6% of 1,091 control cysts; see Fig. 6g). Interestingly, V12Rac1 cells also have defective tight junctions[13], and V12Rac1 cysts formed multiple lumina after 7–9 days in culture (not shown). Exogenous laminin did not affect control cyst development (Fig. 6k, and not shown).

We next investigated the effects of elastase-generated fragments of laminin on N17Rac1 cyst morphogenesis. Elastase cleaves laminin into well-characterized fragments, leaving known receptor-binding sites intact while eliminating the ability of laminin to polymerize[6]. In contrast to native laminin, elastase-digested laminin (ED laminin) did not rescue the N17Rac1 phenotype, even

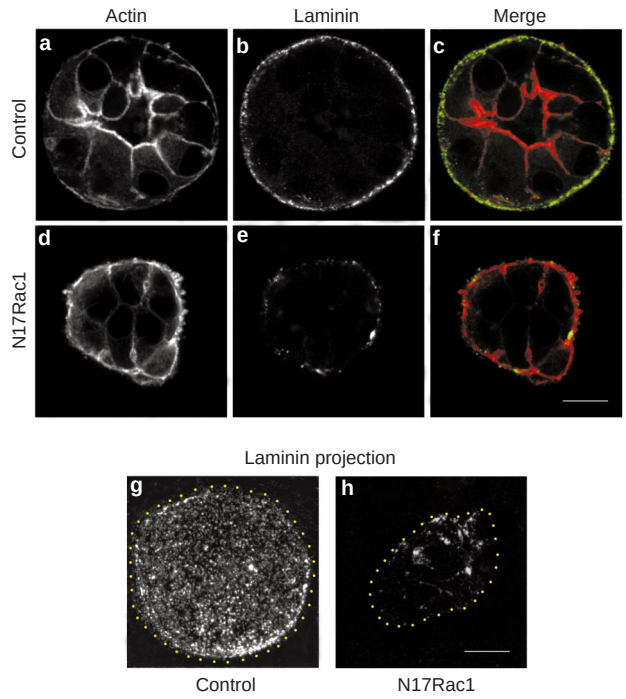

Figure 5 **Abnormal organization of laminin on the surface of N17Rac1 cysts.** Immunocytochemical analysis of laminin deposition on the surface of 4-day control cysts (**a–c**, **g**) and N17Rac1 cysts (**d–f**, **h**). Cysts were stained for actin (**a**, **d**) and laminin (**b**, **e**). The merged images are also shown (**c**, **f**). **a–c**, Laminin completely surrounds control cysts with a punctate, regular distribution. **d–f**, By comparison, laminin on the N17Rac1 cyst surface appears as a few, sparsely distributed patches. **g**, **h**, Projections of confocal sections further contrast the uniform laminin deposition of control cysts with the irregular laminin deposition of N17Rac1 cysts. Yellow dots denote cyst boundaries. Scale bars, 10 μm.

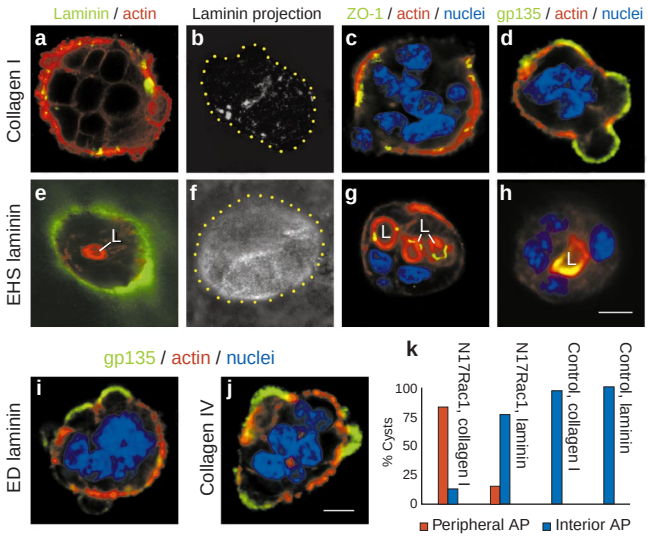

Figure 6 **Exogenous laminin restores proper apical orientation to N17Rac1 cysts. a**, **e**, Apparent recruitment of exogenous laminin to the N17Rac1 cyst surface. N17Rac1 cysts were grown in either collagen alone or collagen supplemented with exogenous laminin-1. After 4 days, cysts were stained for laminin (green) and actin (red). A halo of laminin staining surrounds N17Rac1 cysts in mixed laminin/collagen gels but not cysts in collagen alone. A lumen (L) is visible in the interior of the cyst in **e**. **b**, **f**, Projections of serial confocal sections reveal extensive laminin staining on the surface of N17Rac1 cysts in mixed laminin/collagen gels. This staining contrasts with the sparse, irregular staining of laminin patches on N17Rac1 cysts in collagen alone. Yellow dots denote cyst boundaries. **c**, **d**, **g**, **h**, Exogenous laminin restores normal polarity to N17Rac1 cysts. N17Rac1 cysts were grown in the presence or absence of exogenous laminin. After 4 days, cysts were stained for apical domain markers (green), actin (red), and nuclei (blue). In mixed laminin/collagen gels, N17Rac1 cysts form lumina (L) and an interior apical pole as revealed by the staining of actin, ZO-1 and gp135. In collagen I alone, N17Rac1 cysts do not form lumina and position the apical pole at the cyst periphery. Scale bar, 10 μm. **i**, **j**, The presence of elastase-digested (ED) laminin or collagen IV does not rescue the polarity of N17Rac1 cysts. Scale bar, 10 μm. **k**, Quantification of cyst phenotypes. In collagen I alone, 83% of N17Rac1 cysts exhibited a peripheral apical pole (AP) and 14% exhibited an interior AP (n = 657). In exogenous laminin, only 15% of N17Rac1 cysts exhibited a peripheral AP, whereas 75% exhibited an interior AP, indicating rescue (n = 2,062). These proportions resemble those of control cysts in collagen I alone; 0% of control cysts in collagen exhibited a peripheral AP and 96% exhibited an interior AP (n = 595). Laminin did not significantly alter apical polarization of control cysts because 99% of these cysts exhibited an interior AP and 0% exhibited a peripheral AP (n = 1,091). The sum of cysts with peripheral and interior APs is typically less than 100% because cysts with no or ambiguous APs were also observed. Cysts were scored from four separate experiments with at least 150 cysts per experiment.

at 600 μg ml^{-1} (Fig. 6i). This result is consistent with a requirement for laminin assembly and indicates that receptor ligation alone might be inadequate.

Last, we investigated the ability of other ECM components to rescue the apical orientation of N17Rac1 cysts. Matrigel, a reconstituted basement-membrane mixture primarily containing laminin-1 and collagen type IV, reorientated apical polarity and restored lumen formation to N17Rac1 cysts, as expected (not shown). The laminin component of Matrigel probably effected this rescue because collagen IV alone (1.5 mg ml^{-1}) did not alter N17Rac1 cyst development (Fig. 6j). Finally, the mesenchymal ECM component fibronectin (1.5 mg ml^{-1}) also failed to rescue (not shown). Matrigel, collagen type IV, and fibronectin did not alter control cyst morphogenesis (not shown). Taken together, these results indicate that the orientation of apical polarity is specific to laminin.

In summary, we determined the effects of exogenous laminin on N17Rac1 cyst development. When grown in laminin/collagen gels, N17Rac1 cysts were uniformly surrounded by laminin staining. These cysts polarized normally and developed lumina, whereas cysts grown in the presence of elastase-digested laminin or other ECM components did not. The sufficiency of exogenous laminin to rescue N17Rac1 cyst development implies a causal link between laminin misassembly and apical inversion.

Discussion

In a multicellular tissue, the asymmetry of individual cells must conform to the higher-order tissue architecture. How a cell establishes an axis of polarity that reflects the organization of its parent tissue remains poorly understood. Here we provide evidence for an autocrine loop in which cells create their own extracellular polarity cue during cyst morphogenesis (Fig. 7a). Specifically, we find that intracellular Rac1 controls extracellular laminin assembly. Assembled laminin then acts back on the cell to direct the orientation of the interior apical pole. Blocking Rac1 activity disrupts the loop by impairing laminin assembly because the misassembled laminin is incompetent to signal. The absence of laminin signalling leads to an inversion of the apical pole (Fig. 7b). Taken together, the results illustrate how assembled laminin, the major component of epithelial basement membranes, couples apical polarization to epithelial tissue organization.

Assembled laminin sends a transcellular, polarizing signal. Intracellular Rac1 probably regulates extracellular laminin assembly

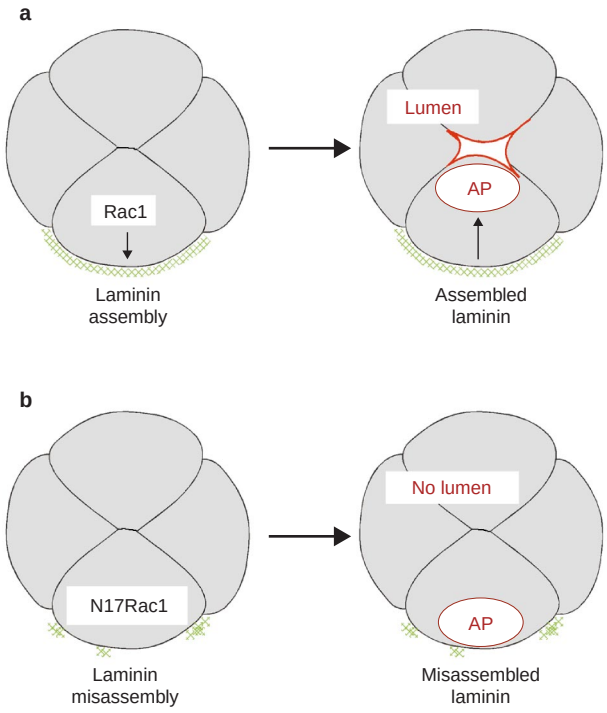

Figure 7 **Model. a**, An autocrine loop orientates apical polarity during normal cyst development. Intracellular Rac1 activity regulates extracellular laminin assembly. Assembled laminin reciprocally acts back on the cell, initiating a transcellular signal that relays positional information to the site of apical pole formation (AP). **b**, Disruption of the autocrine loop inverts apical polarity. N17Rac1 disrupts the assembly of laminin, rendering it incompetent to initiate a polarizing signal. Without this positional information, the developing cyst inverts placement of the AP.

through effects on transmembrane receptors. Numerous studies of assembly have established a central role for dystroglycan and β_1 integrins, including the $\alpha_3\beta_1$ integrin[5,23,25]. Intriguingly, levels of α_3 integrin are decreased by 68% in N17Rac1 cysts, perhaps leading to the impairment of laminin assembly. Decreased α_3 levels persist in cysts rescued by exogenous laminin (not shown), which is consistent with a role upstream of laminin assembly. Rac1 could also modulate the activity of laminin receptors by regulating actin–receptor interactions. Notably, integrins and dystroglycan both form complexes with actin[27,28], and actin filaments are indispensable for laminin assembly[6].

Exogenous laminin is recruited to the cyst surface and restores correct polarity, indicating that it compensates for the impaired signalling of endogenous laminin. Because of its relative abundance, exogenous laminin might drive its own assembly through mass action, overcoming the decrease in α_3 integrin level. Indeed, recruitment and assembly of exogenous laminin have been observed previously with embryonic stem cells and myotubes[5,6]. Exogenous laminin could also nucleate the polymerization of endogenous laminin[29]. Interestingly, the intensity of staining of exogenous laminin diminished rapidly beyond the immediate vicinity of the cysts, despite the abundance of laminin in the gel. This observation is consistent with our earlier proposal that only laminin assembled on the surface of the cyst is detected efficiently by immunofluorescence.

The polarizing signal initiated by laminin must be transmitted across the cell to the eventual site of apical pole formation. Distal elements of this pathway probably include receptors that interpret the laminin signal, receptor-associated cytoskeletal elements that propagate the signal transcellularly, and a spatial cue that ultimately dictates the site of apical pole establishment. Studies of cellularization during *Drosophila* embryogenesis have identified two groups of junctional proteins that might act as apical spatial cues: Bazooka and DaPKC, and Crumbs, Scribble and Discs Lost[3]. Whether their vertebrate homologues form analogous pathways remains to be seen. Notable differences can be found between apical polarization in flies and mammals; in particular, apical polarity during *Drosophila* cellularization does not seem to require laminin[30], and apical polarity in MDCK cells does not require cell–cell junctions, at least when cells are grown on culture supports[4]. Given these discrepancies, further investigation of polarization in these two systems will be of great interest.

N17Rac1 cysts invert the axis of apical polarization. The apical pole of N17Rac1 cysts is consistently inverted towards the cyst periphery. This phenotype contrasts with the loss or randomization of polarity that is frequently observed when regulation of polarization is disrupted in other contexts[10,31–33]. It also underscores the independent natures of pole formation and pole orientation. Indeed, N17Rac1 cysts are unprecedented in placing the apical domain at the cell–ECM interface; in all other reported circumstances, epithelial cells invariably place the apical domain at the free cellular surface[4,19,34].

Inversion of the apical domain could reflect the positioning of the apical cue at the cyst periphery. When grown in suspension culture, normal MDCK cells form cysts with inverted polarity[19]. Laminin accumulates in the interior of these suspension-grown cysts and seems to be involved in polarization[35]. Perhaps an analogous mechanism applies to the N17Rac1 cysts, although we did not detect laminin in the N17Rac1 cyst interior. More likely, the normal, interior apical cue is absent from N17Rac1 cysts, uncovering a subordinate cue that positions the apical domain at the cyst periphery. Such hierarchies have been reported recently in *Drosophila* neuroepithelia and *Caenorhabditis elegans* embryos, in which loss of the dominant cue (the adenomatous polyposis coli protein and sperm asters, respectively) specifically reorientates polarity toward a secondary cue (Bazooka and the meiotic spindle)[36,37].

Although N17Rac1 perturbs the polarity of cysts in collagen, it does not perturb the polarity of monolayers on synthetic supports or cysts in suspension. This finding indicates that different mechanisms might orientate polarity in different extracellular contexts. Both monolayer and suspension culture are inherently anisotropic, providing cells with free and adhesive cellular surfaces. We propose that N17Rac1 cells polarize normally in these circumstances because they receive overriding positional information from the asymmetry of their environment. Conversely, cells in collagen experience an isotropic environment in which all cell surfaces are adhesive, either to collagen or to other cells. These cells must break the symmetry of their environment and polarize without external cues by forming a free luminal surface. In this respect, collagen culture uniquely recapitulates epithelial development *in vivo*. N17Rac1 interferes with symmetry-breaking, resulting in the inverted phenotype of N17Rac1 cysts. Thus, cyst development in collagen reveals a role for Rac1 that is not apparent in simpler, less physiological systems.

The multicellular nature of tissue development requires that the polarity of each individual cell be coordinated with neighbouring cells and the extracellular environment. Our results reveal how the structural features of a tissue can couple the polarity of individual cells to the higher-order tissue architecture. Linking apical orientation to the generation of the basement membrane ensures the proper localization of the apical pole during epithelial cyst development. In this autocrine manner, epithelial cells influence their own morphogenesis by actively modifying their extracellular environment. The identification of Rac1 and laminin as two elements in a common pathway orientating apical polarity provides a basis on which to explore further the molecular mechanisms that control epithelial polarization. □

Methods

Antibodies and reagents.

Immunocytochemistry was performed as described below with the following reagents. Primary antibodies used were mouse anti-*cis*-Golgi enzyme GM130 (Transduction Laboratories), mouse anti-p58 (kind gift of Karl Matlin), mouse anti-E-cadherin (Transduction Laboratories), affinity-purified rabbit anti-laminin (Sigma), rat anti-ZO-1 (R40.76; a gift from Bruce Stevenson), mouse anti-gp135 (a gift from George Ojakian), mouse anti-vimentin (Sigma), mouse anti-α-dystroglycan (Upstate Biotechnology), rabbit anti-α_3 integrin (Chemicon), rabbit anti-α_4 integrin (Chemicon), rat anti-α_6 integrin (GoH3; Serotec) and rat anti-β_1 integrin (AIIB2; a gift from Caroline Damsky). The rabbit anti-laminin antibody (Sigma) was raised against intact laminin-1, consisting of laminin α1, β1 and γ1 chains. Although MDCK cells are known to express laminin-1 (ref. 38), they might also express other variants, such as laminin-10, that contain these chains. Such variants would also have been detected by the anti-laminin antibody. Secondary antibodies used were goat anti-mouse Alexa Fluor 488, goat anti-rat Alexa Fluor 488, goat anti-rabbit Alexa Fluor 488 (all from Molecular Probes), donkey anti-mouse Cy5, sheep anti-mouse horseradish peroxidase (HRP), donkey anti-rabbit HRP and donkey anti-rat HRP (all from Jackson Immunochemicals). Actin filaments were stained with Alexa Fluor 594 phalloidin (Molecular Probes) at a dilution of 1:40. Nuclei were stained with TO-PRO3 (Molecular Probes) at a dilution of 1:100.

Cell culture.

T23 MDCK cells expressing N17Rac1 or V12Rac1 under control of the tetracycline-repressible transactivator have been described extensively elsewhere[12]. Cell lines were maintained in MEM supplemented with 10% FCS, 20 ng ml^{-1} doxycycline, 100 i.u. ml^{-1} penicillin and 100 mg ml^{-1} streptomycin at 37 °C in a humidified atmosphere containing 5% CO_2. To induce exogenous gene expression, 20 ng ml^{-1} doxycycline was removed by washing cells with PBS$^+$ three times immediately before embedding them in collagen I.

Growth of cysts in three-dimensional collagen I gels was performed as described previously[18]. In brief, a suspension of single MDCK cells was added to a solution of buffered, liquefied collagen I. Initial concentrations of 2×10^4 cells ml^{-1} and 2×10^6 cells ml^{-1} was used for immunofluorescence and biochemical experiments, respectively. Cyst development proceeded identically at both concentrations. The final concentration of collagen I in the solution was 2 mg ml^{-1}, allowing the collagen I to solidify into a gel by incubation in a 37 °C oven before the addition of medium. After solidifying, the cultures received medium containing either 20 ng ml^{-1} doxycycline (control conditions in which exogenous gene expression is repressed) or 0–10 ng ml^{-1} doxycycline (to induce exogenous gene expression). Over a 4-day period, individual cells in the collagen I matrix proliferated to form cysts, with each cyst arising from a single cell. Four-day control cysts contained an average of 13. 1 ± 3.4 cells and their average diameter was 56.9 ± 6.9 μm ($n = 10$). Four-day N17Rac1 cysts contained an average of 11.6 ± 4.5 cells and their average diameter was 42.4 ± 11.3 μm ($n = 10$). After 4 days in culture, cysts were processed for either immunocytochemical or biochemical analysis as detailed below.

As described previously[12], in the complete absence of doxycycline, N17Rac1 levels were detected at 20% of endogenous Rac1 levels after 12 h of induction and increased to a maximum of 600% of endogenous Rac1 levels after 48 h. The development of transfected cysts in the presence of 20 ng ml^{-1} doxycycline was indistinguishable from that of untransfected cysts in either the presence or the absence of 20 ng ml^{-1} doxycycline (not shown). All N17Rac1-expressing cysts shown in figures were grown in the absence of doxycycline; however, a comparable phenotype was obtained with lower doxycycline concentrations (4–200 pg ml^{-1}), which substantially diminished N17Rac1 expression[12].

Growth of cells in gels containing collagen I mixed with additional ECM components was performed as for gels containing collagen I alone, with the following differences. For collagen I/laminin mixtures, laminin-1 purified from EHS tumour cell cultures (Becton–Dickinson) was added to collagen I at a final laminin concentration of 250 μg ml^{-1}. For collagen I/elastase-digested laminin mixtures, laminin was purified from the EHS tumour and digested with elastase as described previously[39]. The elastase-digested laminin was added to collagen I at a final laminin concentration of 600 μg ml^{-1}. For collagen I/collagen IV mixtures, collagen IV from the EHS tumour in 0.05 M HCl (Becton–Dickinson) was dialysed overnight at 4 °C against PBS$^+$ and added to collagen I at a final collagen IV concentration of 1.5 mg ml^{-1}. For collagen I/fibronectin mixtures, fibronectin from human plasma in 100 mM 3-(cyclohexylamino)propane-1-sulphonic acid, 0.15 M NaCl, 1 mM $CaCl_2$, pH 11.5 (Becton–Dickinson) was dialysed overnight at 4 °C against PBS$^+$ and added to collagen I at a final fibronectin concentration of 1.5 mg ml^{-1}. After the addition of cells, the solutions were allowed to solidify for 60–90 min in an oven at 37 °C.

To grow cells as monolayers, cells were plated at a density of 2.5×10^5 cells cm^{-2} on 12-mm Transwell polycarbonate filters (0.4 μm pore size; Corning Costar) and grown for 4–7 days with changes of medium every 2 days. To grow cysts in suspension, the wells of a 24-well plate were first coated with Sea Plaque GTG low-melting-point agarose (1% w/v in PBS$^+$) (FMC Bioproducts). After the agarose had solidified, cells were added to the wells at a density of 2×10^4 cells cm^{-2}. Suspension cysts were allowed to grow for 3–7 days with changes of medium every 2 days. In both monolayer and suspension culture, N17Rac1 expression was induced when cells were initially plated.

Immunofluorescence and electron microscopy.

Cysts in gels of collagen I were processed for immunofluorescence as described previously[18], with the following modifications. Before fixation, gels were briefly treated with collagenase type VII (Sigma C-2399) at 100 U ml^{-1} in PBS$^+$ for 15 min at 37 °C to increase the accessibility of antibodies to cysts. After postfixing, nuclei were stained by incubating gels with a 1:100 dilution of TO-PRO3 (Molecular Probes) in PBS$^+$ at 37 °C for 1 h. Samples were then mounted in ProLong (Molecular Probes). Cysts in gels of collagen I mixed with other ECM components were processed similarly, except that samples were digested with collagenase VII for 5 min at 37 °C instead of 15 min.

To stain cysts for extracellular laminin, anti-laminin antibody was diluted in medium and added directly to live cells at 37 °C for 1.5–4 h. To verify that only extracellular antigens were revealed, antibodies against vimentin, an intracellular antigen, were also included; the absence of vimentin staining indicated that laminin staining exclusively represented secreted laminin. Samples were then washed extensively and subjected to the immunofluorescence protocol described above.

Cells grown on filters were processed for immunofluorescence as described previously[40], with the following modification: after postfixing, nuclei were stained by incubating cells with a 1:1,000 dilution of TO-PRO3 for 30 min at 37 °C and then mounted in ProLong.

Cysts in suspension were processed for immunofluorescence as follows. Cysts were pelleted by centrifugation at 700*g* for 5 min and resuspended in Sea Plaque GTG low-melting-point agarose (1 mg ml^{-1} in PBS$^+$) at 37 °C. The cyst/agarose mixture was plated on tissue-culture inserts (Nunc) and left to solidify for 5–10 min at room temperature. Cysts were then fixed in 4% paraformaldehyde for 30 min and processed for immunofluorescence similarly to cysts in collagen type I gels.

For electron microscopy, collagen-grown cysts were fixed in a solution containing 2% glutaraldehyde, 0.8% paraformaldehyde and 0.1 M cacodylate. The cells were stained with osmium and imidazole as described previously[41], then dehydrated, embedded in resin, sectioned and imaged (Zeiss 10CA).

Confocal microscopy, image analysis and quantification of cyst phenotypes.

Cells were viewed with a krypton–argon laser (488 and 564 lines) and a helium-neon laser (633 line) in conjunction with a Bio-Rad 1024 confocal laser scan head attached to either a Nikon Eclipse TE300 microscope or a Nikon Diaphot 200 microscope. Digital images of optical sections of cysts were collected in the *x*–*y* plane of the sample by using a Plan Apo 60× 1.40 numerical aperture (NA) objective coupled with a 3× zoom. Digital images of optical sections of monolayers were collected in the *x*–*z* plane of the sample with a Plan Apo 100× 1.40 NA objective. For projections, a stack of images representing one-half of a cyst was collected at 0.5 μm intervals. Images were converted from Bio-Rad PIC format to TIFF format and analysed with NIH Image 1.61 software. Images for figures were colourized, resized, arranged and labelled with Adobe Photoshop 5.0 software.

For the quantification of cyst phenotypes, cysts were stained for actin, nuclei and gp135 as described above. Samples were viewed with epifluorescence and cysts were classified as possessing an interior apical pole, a peripheral apical pole or an ambiguous apical pole on the basis of the following criteria: cysts with intense staining of actin and gp135 at either an interior luminal surface or at cell–cell contacts were considered to have an interior apical pole; cysts with intense staining of actin and gp135 at the cyst–substratum interface were considered to have a peripheral apical pole; cysts that lacked intense staining of actin and detectable gp135 and cysts that exhibited these two markers both in the cyst interior and at the cyst–substratum interface were considered to have an ambiguous apical pole. Whether a cyst possessed either one or more than one lumen was also recorded.

Biochemical analysis of cysts.

To prepare solubilized gel samples, cyst-containing collagen gels were incubated in SDS lysis buffer (0.5% SDS, 100 mM NaCl, 50 mM TEA-Cl pH 8.1, 5 mM EDTA pH 8.0, 0.2% NaN_3 plus protease inhibitor cocktail (5 mg ml^{-1} pepstatin, 10 mg ml^{-1} chymostatin, 5 mg ml^{-1} leupeptin, 50 mg ml^{-1} antipain, 500 mM benzamidine, 10 i.u. ml^{-1} aprotinin and 1 mM PMSF)) for 15 min at 70 °C. This treatment denatured the collagen matrix and lysed the cysts. A small fraction of the solubilized mixture was set aside to determine protein concentrations and the remainder was used for immunoprecipitation.

To prepare lysates, cysts were first isolated from collagen gels as follows. Cyst-containing collagen gels were incubated in MEM containing 4,000 U ml^{-1} collagenase (Sigma C-0773), 0.005% DNase (Boehringer) and protease inhibitor cocktail (to inhibit protease contaminants in the collagenase) for 45 min at 37 °C with gentle rotation to digest the collagen matrix. In some cases, protease inhibitors were omitted and 8.3 mg ml^{-1} trypsin (Worthington) was included to digest extracellular proteins. After digestion, trypsin was inhibited with *N*-tosyl-L-leucine chloromethyl ketone at a final concentration of 0.2 mg ml^{-1} (Boehringer). Intact cysts were then pelleted from the collagenase-treated mixture by centrifugation at 3,000*g* for 3 min, and washed twice with PBS$^+$ to remove residual collagen. After washing, a small fraction of the cyst pellet was set aside to determine protein concentrations. The remainder of the cyst pellet was either lysed in sample buffer (for direct immunoblotting) or lysed in SDS lysis buffer (for immunoprecipitation) and heated at 70 °C for 10 min to inactivate intracellular proteases.

For immunoblotting of cyst lysates, protein concentrations in different lysates were normalized on the basis of the results of a bicinchoninic acid (BCA) protein assay. Normalization by cell number (DNA content as determined by a CyQuant assay (Molecular Probes)) produced relative values within 5% of those obtained with normalization by BCA. Lysates were analysed by reducing SDS–PAGE with 12% gels (for Rac1 and vimentin) or 3–8% gradient gels (for laminin and laminin receptors), followed by immunoblotting.

For immunoprecipitation from cyst lysates and solubilized gels, Triton X-100 was added to samples at a final concentration of 1.67%. For immunoprecipitation from medium, SDS was added to a final concentration of 0.5% and the samples of medium were heated at 70 °C for 10 min before the addition of Triton X-100. All samples were precleared with CL2B beads (Pharmacia) before the addition of 1 μl primary antibody. Samples were incubated with primary antibody overnight at 4 °C with gentle rotation. Subsequently, samples were incubated with ~20 μl Protein G- or Protein A-conjugated Sepharose beads (Pharmacia) for 1 h at room temperature, with rotation. The beads were washed before resuspension in sample buffer with 0.1 M dithiothreitol. Immunoprecipitates were analysed by reducing SDS–PAGE and immunoblotted in a similar manner to to cyst lysates.

RECEIVED 14 JUNE 2000; REVISED 11 APRIL 2001, ACCEPTED 7 JUNE 2001;
PUBLISHED 17 AUGUST 2001.

1. Drubin, D. G. & Nelson, W. J. Origins of cell polarity. *Cell* **84,** 335–344 (1996).
2. Bryant, P. J. & Huwe, A. LAP proteins: what's up with epithelia? *Nature Cell Biol.* **2,** E141–E143 (2000).
3. Knust, E. Control of epithelial cell shape and polarity. *Curr. Opin. Genet. Dev.* **10,** 471–475 (2000).
4. Vega-Salas, D. E., Salas, P. J., Gundersen, D. & Rodriguez-Boulan, E. Formation of the apical pole of epithelial (Madin–Darby canine kidney) cells: polarity of an apical protein is independent of tight junctions while segregation of a basolateral marker requires cell–cell interactions. *J. Cell Biol.* **104,** 905–916 (1987).
5. Henry, M. D. & Campbell, K. P. A role for dystroglycan in basement membrane assembly. *Cell* **95,** 859–870 (1998).
6. Colognato, H., Winkelmann, D. A. & Yurchenco, P. D. Laminin polymerisation induces a receptor–cytoskeleton network. *J. Cell Biol.* **145,** 619–631 (1999).
7. Klinowska, T. C. *et al.* Laminin and β1 integrins are crucial for normal mammary gland development in the mouse. *Dev. Biol.* **215,** 13–32 (1999).
8. Schuger, L., Yurchenco, P., Relan, N. K. & Yang, Y. Laminin fragment E4 inhibition studies: base-

ment membrane assembly and embryonic lung epithelial cell polarisation requires laminin polymerisation. *Int. J. Dev. Biol.* **42,** 217–220 (1998).
9. Williamson, R. A. *et al.* Dystroglycan is essential for early embryonic development: disruption of Reichert's membrane in Dag1-null mice. *Hum. Mol. Genet.* **6,** 831–841 (1997).
10. Kroschewski, R., Hall, A. & Mellman, I. Cdc42 controls secretory and endocytic transport to the basolateral plasma membrane of MDCK cells. *Nature Cell Biol.* **1,** 8–13 (1999).
11. Takaishi, K., Sasaki, T., Kotani, H., Nishioka, H. & Takai, Y. Regulation of cell–cell adhesion by rac and rho small G proteins in MDCK cells. *J. Cell Biol.* **139,** 1047–1059 (1997).
12. Jou, T. S. & Nelson, W. J. Effects of regulated expression of mutant RhoA and Rac1 small GTPases on the development of epithelial (MDCK) cell polarity. *J. Cell Biol.* **142,** 85–100 (1998).
13. Jou, T. S., Schneeberger, E. E. & Nelson, W. J. Structural and functional regulation of tight junctions by rhoA and rac1 small GTPases. *J. Cell Biol.* **142,** 101–115 (1998).
14. McAteer, J. A., Dougherty, G. S., Gardner, K. D. Jr & Evan, A. P. Polarised epithelial cysts *in vitro*: a review of cell and explant culture systems that exhibit epithelial cyst formation. *Scanning Microsc.* **2,** 1739–1763 (1988).
15. Hagios, C., Lochter, A. & Bissell, M. J. Tissue architecture: the ultimate regulator of epithelial function? *Phil. Trans. R. Soc. Lond. B* **353,** 857–870 (1998).
16. Schwimmer, R. & Ojakian, G. K. The α2β1 integrin regulates collagen-mediated MDCK epithelial membrane remodelling and tubule formation. *J. Cell Sci.* **108,** 2487–2498 (1995).
17. Zuk, A. & Matlin, K. S. Apical β1 integrin in polarised MDCK cells mediates tubulocyst formation in response to type I collagen overlay. *J. Cell Sci.* **109,** 1875–1889 (1996).
18. Pollack, A. L., Runyan, R. B. & Mostov, K. E. Morphogenetic mechanisms of epithelial tubulogenesis: MDCK cell polarity is transiently rearranged without loss of cell–cell contact during scatter factor/hepatocyte growth factor-induced tubulogenesis. *Dev. Biol.* **204,** 64–79 (1998).
19. Wang, A. Z., Ojakian, G. K. & Nelson, W. J. Steps in the morphogenesis of a polarised epithelium. I. Uncoupling the roles of cell–cell and cell–substratum contact in establishing plasma membrane polarity in multicellular epithelial (MDCK) cysts. *J. Cell Sci.* **95,** 137–151 (1990).
20. Ekblom, M., Falk, M., Salmivirta, K., Durbeej, M. & Ekblom, P. Laminin isoforms and epithelial development. *Ann. N.Y. Acad. Sci.* **857,** 194–211 (1998).
21. Yang, Y., Palmer, K. C., Relan, N., Diglio, C. & Schuger, L. Role of laminin polymerisation at the epithelial mesenchymal interface in bronchial myogenesis. *Development* **125,** 2621–2629 (1998).
22. Lallier, T., Artinger, M., Matthew, W. & Bronner-Fraser, M. Distribution and biochemical characterisation of the INO antigen during chick neural crest cell migration. *Neurosci. Res. Suppl.* **13,** S126–S140 (1990).
23. Henry, M. D. *et al.* Distinct roles for dystroglycan, β1 integrin and perlecan in cell surface laminin organization. *J. Cell Sci.* **114,** 1137–1144 (2001).
24. Schoenenberger, C. A., Zuk, A., Zinkl, G. M., Kendall, D. & Matlin, K. S. Integrin expression and localisation in normal MDCK cells and transformed MDCK cells lacking apical polarity. *J. Cell Sci.* **107,** 527–541 (1994).
25. DiPersio, C. M., Hodivala-Dilke, K. M., Jaenisch, R., Kreidberg, J. A. & Hynes, R. O. α3β1 integrin is required for normal development of the epidermal basement membrane. *J. Cell Biol.* **137,** 729–742 (1997).
26. Yap, A. S., Stevenson, B. R., Armstrong, J. W., Keast, J. R. & Manley, S. W. Thyroid epithelial morphogenesis *in vitro*: a role for bumetanide-sensitive Cl^- secretion during follicular lumen development. *Exp. Cell Res.* **213,** 319–326 (1994).
27. Ervasti, J. M. & Campbell, K. P. A role for the dystrophin–glycoprotein complex as a transmembrane linker between laminin and actin. *J. Cell Biol.* **122,** 809–823 (1993).
28. Yamada, K. M. & Geiger, B. Molecular interactions in cell adhesion complexes. *Curr. Opin. Cell Biol.* **9,** 76–85 (1997).
29. Cheng, Y. S., Champliaud, M. F., Burgeson, R. E., Marinkovich, M. P. & Yurchenco, P. D. Self-assembly of laminin isoforms. *J. Biol. Chem.* **272,** 31525–31532 (1997).
30. Brown, N. H., Gregory, S. L. & Martin-Bermudo, M. D. Integrins as mediators of morphogenesis in *Drosophila*. *Dev. Biol.* **223,** 1–16 (2000).
31. Bilder, D. & Perrimon, N. Localisation of apical epithelial determinants by the basolateral PDZ protein Scribble. *Nature* **403,** 676–680 (2000).
32. Chant, J. & Herskowitz, I. Genetic control of bud site selection in yeast by a set of gene products that constitute a morphogenetic pathway. *Cell* **65,** 1203–1212 (1991).
33. Kraut, R., Chia, W., Jan, L. Y., Jan, Y. N. & Knoblich, J. A. Role of inscuteable in orienting asymmetric cell divisions in *Drosophila*. *Nature* **383,** 50–55 (1996).
34. Hall, H. G., Farson, D. A. & Bissell, M. J. Lumen formation by epithelial cell lines in response to collagen overlay: a morphogenetic model in culture. *Proc. Natl Acad. Sci. USA* **79,** 4672–4676 (1982).
35. Wang, A. Z., Ojakian, G. K. & Nelson, W. J. Steps in the morphogenesis of a polarised epithelium. II. Disassembly and assembly of plasma membrane domains during reversal of epithelial cell polarity in multicellular epithelial (MDCK) cysts. *J. Cell Sci.* **95,** 153–165 (1990).
36. Lu, B., Roegiers, F., Jan, L. Y. & Jan, Y. N. Adherens junctions inhibit asymmetric division in the *Drosophila* epithelium. *Nature* **409,** 522–525 (2001).
37. Wallenfang, M. R. & Seydoux, G. Polarisation of the anterior–posterior axis of *C. elegans* is a microtubule-directed process. *Nature* **408,** 89–92 (2000).
38. Caplan, M. J. *et al.* Dependence on pH of polarized sorting of secreted proteins. *Nature* **329,** 632–635 (1987).
39. Yurchenco, P. D. & O'Rear, J. J. Basement membrane assembly. *Methods Enzymol.* **245,** 489–518 (1994).
40. Cardone, M. H., Smith, B. L., Song, W., Mochly-Rosen, D. & Mostov, K. E. Phorbol myristate acetate-mediated stimulation of transcytosis and apical recycling in MDCK cells. *J. Cell Biol.* **124,** 717–727 (1994).
41. Thiery, G., Bernier, J. & Bergeron, M. A simple technique for staining of cell membranes with imidazole and osmium tetroxide. *J. Histochem. Cytochem.* **43,** 1079–1084 (1995).

ACKNOWLEDGEMENTS

We thank Sandra Huling and the UCSF Liver Center Core Facility for preparing electron micrographs; Peter Bacchetti for biostatistical support; Joshua Thaler for invaluable discussions and advice; Mirjam Zegers, W. James Nelson, Fay Shamanski, Erin Gensch, Henry Bourne, Cori Bargmann, Yuh-Nung Jan, Zena Werb and Daniel Kalman for a critical reading of the manuscript; and Karl Matlin for stimulating discussions. L.E.O. is the recipient of a National Defense Science and Engineering Graduate Fellowship and of a predoctoral fellowship from the American Heart Association. T.S.J. is supported by the National Science Council. S.H.H. is the recipient of an award from the Weimann Foundation. A.L.P. is supported by a NIH training grant postdoctoral fellowship. P.Y. is supported by a grant from the NIH. This investigation was supported by a DAMD grant and NIH grants to K.E.M.
Correspondence and requests for materials should be addressed to K.E.M.